Supporting Information

Huang *et al.* 10.1073/pnas.0805309105

SI Text

Spring Model of Gram-Negative Cell Wall. The leftmost *Inset* of Fig. 1*A* from the main text, a schematic of the forces acting on each vertex of our spring model of the peptidoglycan network, is reproduced in Fig. S1. The vertex $\mathbf{r}$ (yellow sphere) connects to vertices at $\mathbf{r}_{g1}$ and $\mathbf{r}_{g2}$ via glycan springs with relaxed length l_g and spring constant k_g, and to vertex $\mathbf{r}_p$ via a peptide spring wiith relaxed length l_p and spring constant k_p. The total spring extension force on $\mathbf{r}$ is

$$\mathbf{F}_k(\mathbf{r}) = -k_g\,(|\mathbf{r}-\mathbf{r}_{g1}| - l_g)\,\frac{\mathbf{r}-\mathbf{r}_{g1}}{|\mathbf{r}-\mathbf{r}_{g1}|} - k_g\,(|\mathbf{r}-\mathbf{r}_{g2}| - l_g)\,\frac{\mathbf{r}-\mathbf{r}_{g2}}{|\mathbf{r}-\mathbf{r}_{g2}|} - k_p\,(|\mathbf{r}-\mathbf{r}_p| - l_p)\,\frac{\mathbf{r}-\mathbf{r}_p}{|\mathbf{r}-\mathbf{r}_p|}. \quad [1]$$

To model the tendency of glycans to form straight strands in the absence of crosslinking, we also include the force due to the glycan bending energy E_{bend}

$$\mathbf{F}_{\text{bend}} = \nabla E_{\text{bend}} = \frac{1}{2}\,\nabla[\,\kappa_{gg}(\theta_{g1g2} - \pi)^2 + \kappa_{pg}(\theta_{pg1} - \pi/2)^2 + \kappa_{pg}(\theta_{pg2} - \pi/2)^2]. \quad [2]$$

where ∇ is the gradient with respect to changes in the vertex position $\mathbf{r}$, θ_{ij} is the angle between $\mathbf{r}_i - \mathbf{r}$ and $\mathbf{r}_j - \mathbf{r}$, and κ_{gg} and κ_{pg} are bending spring constants that penalize deviations from π and $\pi/2$, respectively, with $\kappa_{gg} \gg \kappa_{pg}$.

To calculate the forces due to the osmotic pressure differential Π across the cytoplasmic membrane, we first divide each hexagon of the spring network into six triangles defined by the edges of the hexagon and its center of mass. We can then calculate the volume V of the cylinder by summing over the volumes of the prisms defined by the triangles on the surface and the center of the cylinder. The force due to osmotic pressure on a vertex is then $\mathbf{F}_\Pi = \Pi\nabla V$.

Any spring attached to a dangling vertex is removed from the network (k set to zero) since such springs are free to move and hence do not contribute to bearing the osmotic stress. The positions of unconnected vertices are self-consistently determined by the center of mass of their three neighbors for the purpose of defining the cell surface. To prevent artifacts arising from the open ends of the model cell, we do not allow peptide or glycan defects in the four glycan hoops nearest to each end.

In an unstressed Gram-negative cell wall, the typical distance between adjacent peptide crosslinks along a glycan strand is l_g = 2 nm (two disaccharide units), while the end-to-end length of peptides is l_p = 1–1.3 nm (1). An estimate of the effective spring constant of a peptide is $k_p \approx 10^{-2}$ N/m (2). The correlation length of an unbranched glycan strand is much longer (roughly 10 nm) than that of a peptide (≈0.2 nm), such that the glycan strands are much stiffer than the peptide crosslinks (1). To match the anisotropic elastic properties and correlation lengths of the peptidoglycan (4), we modeled the glycan springs with $k_g = 5k_p$ and $l_g = 2l_p$, (except as noted for the defects in Fig. 4*B*), and bending force constants κ_{gg} = 10 pN nm, $\kappa_{pg} = 0$.

Tension Induced by Defects on Surrounding Peptidoglycan. In Fig. 1*A*, we observed that the tension induced by a single peptide or a single glycan defect is isolated to a small neighborhood around the defect. To quantify the range of the perturbation and test its dependence on the size of the cell wall, we studied the response of model cell walls with N_c = 150 hoops of N_g = 50, 100, and 150 glycan units per hoop at finite pressure ($\Pi = 0.01$) to either a single peptide or glycan defect at the center of the cell. In Fig. S2, we plot the increase in extension in each spring relative to the background extension far away from the defect, as a function of the spring's distance from the defect. Because the background extension in springs far away from the defect does depend slightly on N_g, we normalize to this extension for comparison.

In Fig. S2 *A* and *B*, the normalized peptide extension decays to zero with the same pattern regardless of cell circumference ($\propto N_g$), and the range of the perturbation is similar for peptide or glycan defects. The same holds true for the normalized glycan extension in Fig. S2 *C* and *D*, excepting the glycans in the same hoop as a glycan defect which have a slightly longer range of perturbation.

The number of disaccharide units in a hoop with the circumference of an *E. coli* cell is ≈3,000, much larger than in our model cells. However, since the short range of perturbation around each defect is a general property of a 2D spring network independent of its overall size, the observed robustness of cell shape to defects is expected to persist for arbitrarily large model networks.

Simulated Dynamics of Cell Cracking. In Fig. 3, we initialize a model cell wall with small patch of peptide defects near midcell, and then repeatedly remove the 10 peptides under the most tension after the equilibration. The cell cracking shown in Fig. S3 does not depend qualitatively on the number of peptides removed at each step. For $n < 10$, the same pattern of defects results, simply requiring more steps. For $n > 10$, additional peptides are removed further to the left and right of the patch, which accelerates the cracking process but does not alter the series of shapes. Similar cracked shapes arise if all peptides that exceed a critical tension are removed at each step.

In contrast to the single-layered cell wall of Gram-negative bacteria, the cell wall of Gram positive bacteria such as *Bacillus subtilis* is 10-20 layers thick. This increase in thickness permits a higher turgor pressure in *B. subtilis* [≈26 atmospheres (5)], 5- to 10-fold above that in *E. coli*. Nevertheless, the robustness of the Gram-negative cell wall suggests that the rules governing peptidoglycan synthesis may be qualitatively similar in Gram-negative and Gram positive bacteria, i.e., that some degree of breaking before making may be permitted in both cases. In the *B. subtilis* cell wall, the layers of peptidoglycan are presumed to be crosslinked by peptides (6, 7). We found that vancomycin-treated *B. subtilis* cells did not bulge, but rather maintained a rod shape until lysis occurred (data not shown, and see ref.6). In this case, a patch of defects that forms in one layer is unlikely to coincide with the location of defects in other layers, making the cell more resistant to cell-shape changes.

Swelling Is Confined to the Bulge During Cell Cracking. As shown in Fig. S4, we quantified the cross-sectional diameter of the cell, the bulge width, and the cracking angle for 2 typical cells as functions of time. To quantify the morphologies of the vancomycin-treated cells, time-lapse images were imported into Matlab (Mathworks), where cell boundaries were extracted using the contour function. For each cell, a midline was fitted and the cell widths measured at 8 equidistant points along the length of the cell. The angle of cell bending was measured as the angle between the 2

segments of the midline that fitted a bent cell. The width of the bulge was measured from the largest extent of the bulge to the opposite cell boundary.

For both cells, the diameter remained approximately constant, although there was a slight decrease when the bulge formed. This slight decrease in cylindrical diameter is typical in bulging cells. (While this decrease in diameter upon cracking agrees qualitatively with the slight decrease in Fig. 1*B*, the larger magnitude may stem in part from the reduction in the osmotic pressure caused by bulging of the membrane.) As shown in Fig. S4*B*, the cracking angle decreased from 180° to ≈90° as the bulge grew, but the cells retained their cylindrical shapes away from the bulge. The sudden onset of bulging and a sharp drop in the cracking angle is in agreement with our observation that a critical number of peptides must be absent before noticeable cracking occurs in our model cell walls (compare Fig. S3 *C* and *D*). The agreement between the model predictions and experimental results regarding the cylindrical shape of the cells outside of the bulge also further legitimizes the horizontal model for the cell wall of Gram-negative bacteria.

Matching Experimental Glycan Strand-Length Distribution. To generate a model cell wall with a specified peptide defect concentration and a glycan strand-length distribution that agrees with the experimental distribution p_n^{expt} in ref. 8, we first randomly removed peptide crosslinks to reach the desired peptide defect concentration. We then performed Monte Carlo simulations to adjust the glycan strand-length distribution to match experiment. In each Monte Carlo step, 1 of each of 3 types of modifications to the peptidoglycan network were attempted: (*i*) a defect was added by removing an existing glycan spring, (*ii*) a defect was removed by reinstating a glycan spring, or (*iii*) a defect was moved by removing an existing spring and reinstating a spring at a different location. After each attempted move, all dangling springs (at least 1 end with connectivity one) were temporarily removed, and the glycan strand-length distribution was calculated. Each attempted change was accepted only if it reduced the Kullback–Leibler divergence

$$\phi_{KL}[p_n] = \sum_n (p_n + b_n) \log\left(\frac{p_n + b_n}{p_n^{expt} + b_n}\right), \qquad [3]$$

a common measure of the distance between two probability distributions. The use of pseudocounts $b_n = 0.001$ ensures that ϕ_{KL} is finite for all distributions.

The Monte Carlo samplings continued until $\phi_{\text{KL}} < 0.001$. A comparison of the distribution p_n produced by one such simulation (with no initial peptide defects) with p_n^{expt} is shown in Fig. 3*C* and the equilibrated cell wall is shown in the topmost image of Fig. 3*B*. The agreement in the glycan strand-length distributions p_n and p_n^{expt} is similarly good for the other initial peptide-defect concentrations in Fig. 3*B*. In ref. 9, similar glycan strand-length distributions were generated by assuming a set of physical rules governing the interactions between adjacent pores and the consequent formation of glycan defects. In Fig. S5, we show that the cracked cell shapes in Fig. 1 and Fig. S3 are not affected by the addition of the same glycan defects in the topmost image of Fig. 3*B*, with the distribution shown in Fig. 3*C*. We have ignored any glycan defects that would fall within the patch of peptide defects so that the surface of the cell can be sensibly defined (see *Materials and Methods*).

Effect of Turgor Pressure on Cell-Wall Dimensions. In Fig. S6, we plot the dimensions of a model cell wall without defects as a function of the turgor pressure. For the range of pressures shown, the spring network stretches as the turgor pressure increases and both the length and radius increase linearly, with the length increasing at a faster rate. For our chosen values of k_p and l_p, the rate of increase of length is 26% per atmosphere of turgor pressure, comparable to the estimates in ref. 3. However, the cell-wall dimensions are sensitive to the presence and distribution of defects, as noted in the main text (see Fig. 3).

Normal Modes of Cell Shape. To study the normal modes of a defect-free model peptidoglycan network, we write the potential energy of the spring network as a sum of Hooke's Law terms (10):

$$V = \sum_{\langle n,m\rangle} \frac{1}{2} k_{nm} \left(|\mathbf{r}_n - \mathbf{r}_m| - l_{nm}\right)^2, \qquad [4]$$

where the sum is over pairs of vertices $\langle n,m\rangle$ connected by springs and $k_{nm} \in \{k_p,k_g\}$, $l_{nm} \in \{l_p,l_g\}$. The normal modes are obtained by diagonalizing the $3N_cN_g \times 3N_cN_g$ spring matrix $\tilde{K}$ whose elements are

$$\tilde{K}_{nm} = \frac{\partial \mathbf{F}_n}{\partial \mathbf{r}_m}, \qquad [5]$$

where $\mathbf{F}_n = \partial V/\partial \mathbf{r}_n + (\mathbf{F}_\Pi)_n$ and $(\mathbf{F}_\Pi)_n$ is the force exerted by osmotic pressure at $\mathbf{r}_n$. The eigenvalues $\tilde{K}_q$ of $\tilde{K}$ represent effective spring constants for the normal modes, which may be thought of as resonant cell shapes.

The extended normal modes with the smallest nonzero eigenvalues for a cell wall with $N_g = 28$ and $N_c = 36$ are shown in Fig. S7 (zero-eigenvalue modes are translations and rotations of the entire cylinder). The lowest eigenvalue mode, which requires the least energy to excite, is the doubly degenerate bend mode shown in Fig. S7*A*. The next lowest mode shown in Fig. S7*B* is a twist of the cylinder. Higher modes combine increased curvature (as shown in Fig. S7*C*), twist, and asymmetric stretching and compression. A Principal Components Analysis of the shapes that result from single defects yields principal component eigenvectors which are qualitatively the same as the normal modes in Fig. S7.

Misdirected Glycan Synthesis. In Fig. 4*D*, a lemon-shaped cell was produced by randomly replacing glycan springs by an effective spring representing a glycan–peptide–glycan segment with probability $0.1+0.5|1-2z/L|$, where z is the longitudinal distance between the glycan and the middle of a cell of length L. Fig. S8 shows a schematic motivating this replacement. When glycan synthesis, initially occurring along the circumferential direction, becomes misdirected along the longitudinal direction and is then put under stress, peptide springs are incorporated into the hoops. The resulting glycan–peptide–glycan springs in series then behave as an effective spring with a lower spring constant than a glycan spring, making it easier for the cell to swell. This effective spring has a relaxed length $l_p + 2l_g$ and a spring constant $k_pk_g/(2k_p + k_g)$, appropriate for springs in series.

1. Boal D (2002) *Mechanics of the Cell* (Cambridge Univ Press, Cambridge, UK), 1st Ed.
2. Boulbitch A, Quinn B, Pink D (2000) Elasticity of the rod-shaped Gram-negative eubacteria. *Phys Rev Lett* 85:5246–5249.
3. Cros S, Garnier C, Axelos MAV, Imberty A, Pérez S (1996) Solution conformations of pectin polysaccharides: Determination of chain characteristics by small angle neutron scattering, viscometry, and molecular modeling. *Biopolymers* 39:339–352.
4. Yao X, Jericho M, Pink D, Beveridge T (1999) Thickness and elasticity of Gram-negative murein sacculi measured by atomic force microscopy. *J Bacteriol* 181:6865–6875.
5. Thwaites JJ, Surana UC (1991) Mechanical properties of *Bacillus subtillis* cell walls: Effects of removing residual culture medium. *J Bacteriol* 173:197–776.
6. Daniel RA, Errington J (2003) Control of cell morphogenesis in bacteria: Two distinct ways to make a rod-shaped cell. *Cell* 113:767–776.
7. Scheffers DJ, Pinho MG (2005) Bacterial cell wall synthesis: New insights from localization studies. *Microbiol Molec Biol Rev* 69:585–607.
8. Obermann W, Höltje JV (1994) Alterations of murein structure and of penicillin-binding proteins in minicells from *Escherichia coli*. *Microbiology* 140:79–87.
9. Pink D, Moeller J, Quinn B, Jericho M, Beveridge T (2000) On the architecture of the Gram-negative bacterial murein sacculus. *J Bacteriol* 182:5925–5930.
10. Emberley EG, Mukhopadhyay R, Wingreen NS, Tang C (2003) Flexibility of α-helices: Results of a statistical analysis of database protein structures. *J Mol Biol* 327:229–237.

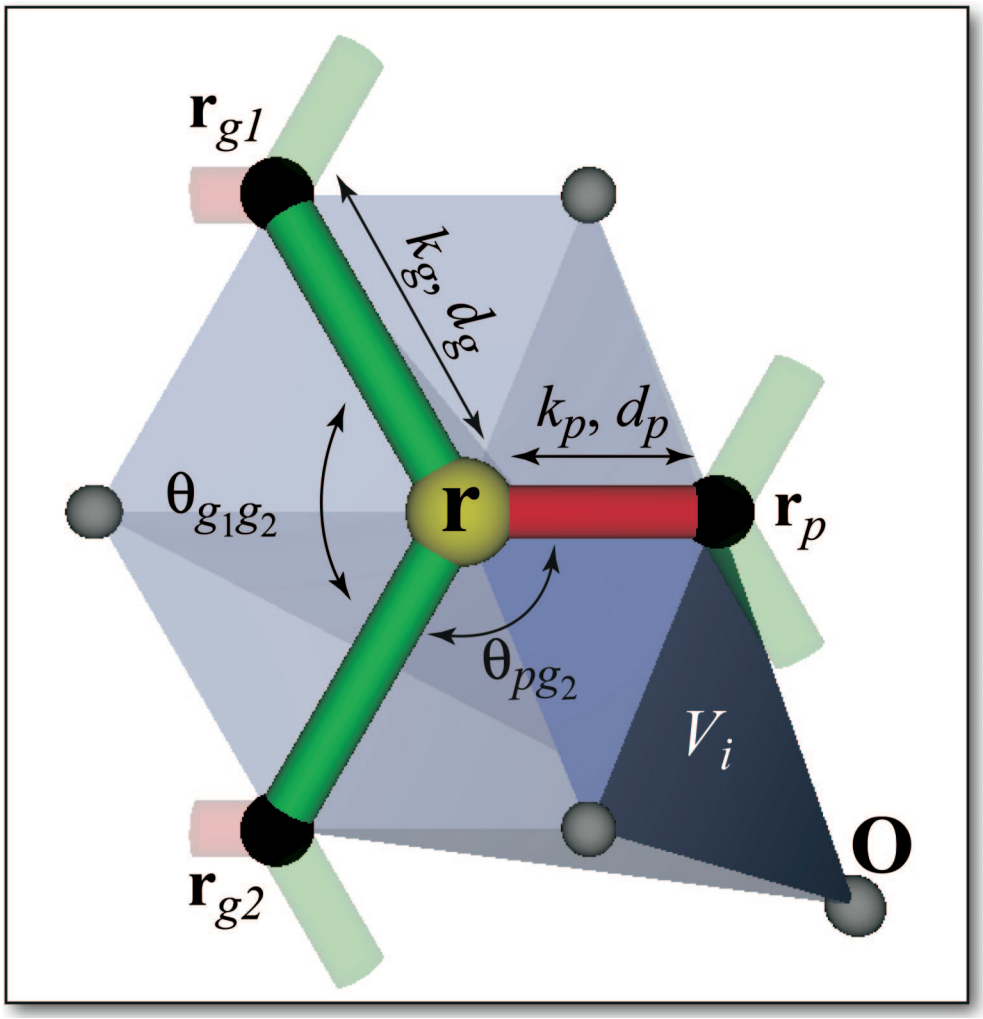

Fig. S1. Spring model for the peptidoglycan cell wall of Gram-negative bacteria. Glycans (green) and peptides (red) are modeled as springs with relaxed lengths l_p,l_g and spring constants k_p, k_g, κ_{gg}, and κ_{pg}. Each vertex links 2 glycan springs and 1 peptide spring. Each hexagon of the spring network is decomposed into triangles (blue) using its center of mass (gray spheres), with the force due to osmotic pressure $\mathbf{F}_\Pi$ on each vertex arising from the 6 adjacent prisms (see Eq. **2**).

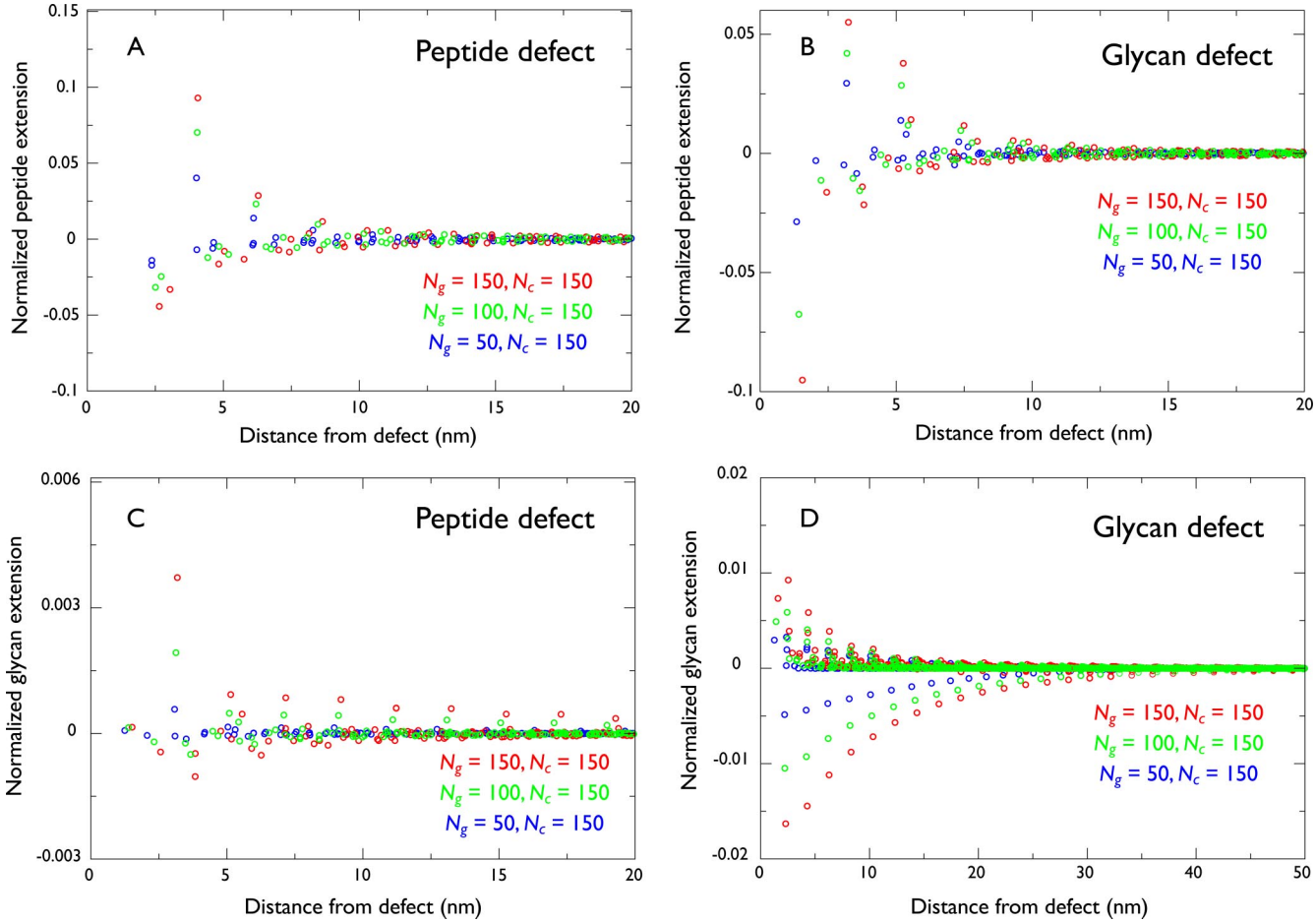

Fig. S2. Single peptidoglycan defects only stretch remaining springs in a small neighborhood, which is independent of overall network size. (*A* and *B*) The normalized peptide extension relative to the background peptide extension as a function of distance from a peptide (*A*) or a glycan (*B*) defect positioned at midcell. The distance over which the defect-induced extension decays is very similar for networks with N_g = 150 (red), 100 (green), or 50 (blue) glycans per hoop, (*C* and *D*) The same as *A* and *B* except showing the normalized glycan extension.

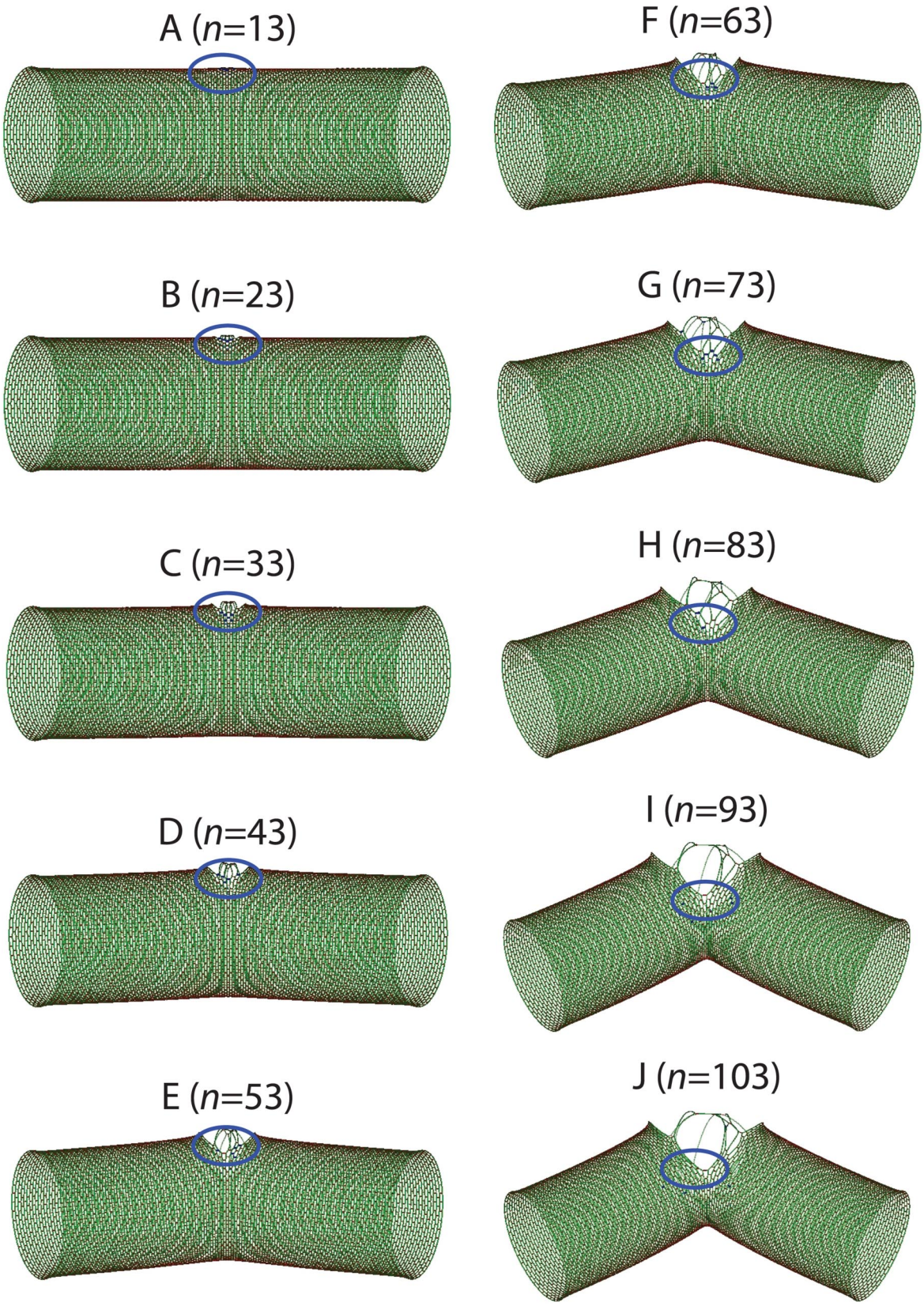

Fig. S3. ''Cracking'' of a cell initiated by 2 neighboring peptide defects near midcell. (*A–J*) At each stage, the 10 peptides under the most tension (blue ovals) are removed. As the number of defects increases from $n = 13$ in *A* to $n = 43$ in *D*, a gap opens at the middle of the cell but the overall cell wall remains nearly cylindrical. As the number of defects increases further, the cell begins to crack and the 2 halves of the cell angle away from the center of the defect patch.

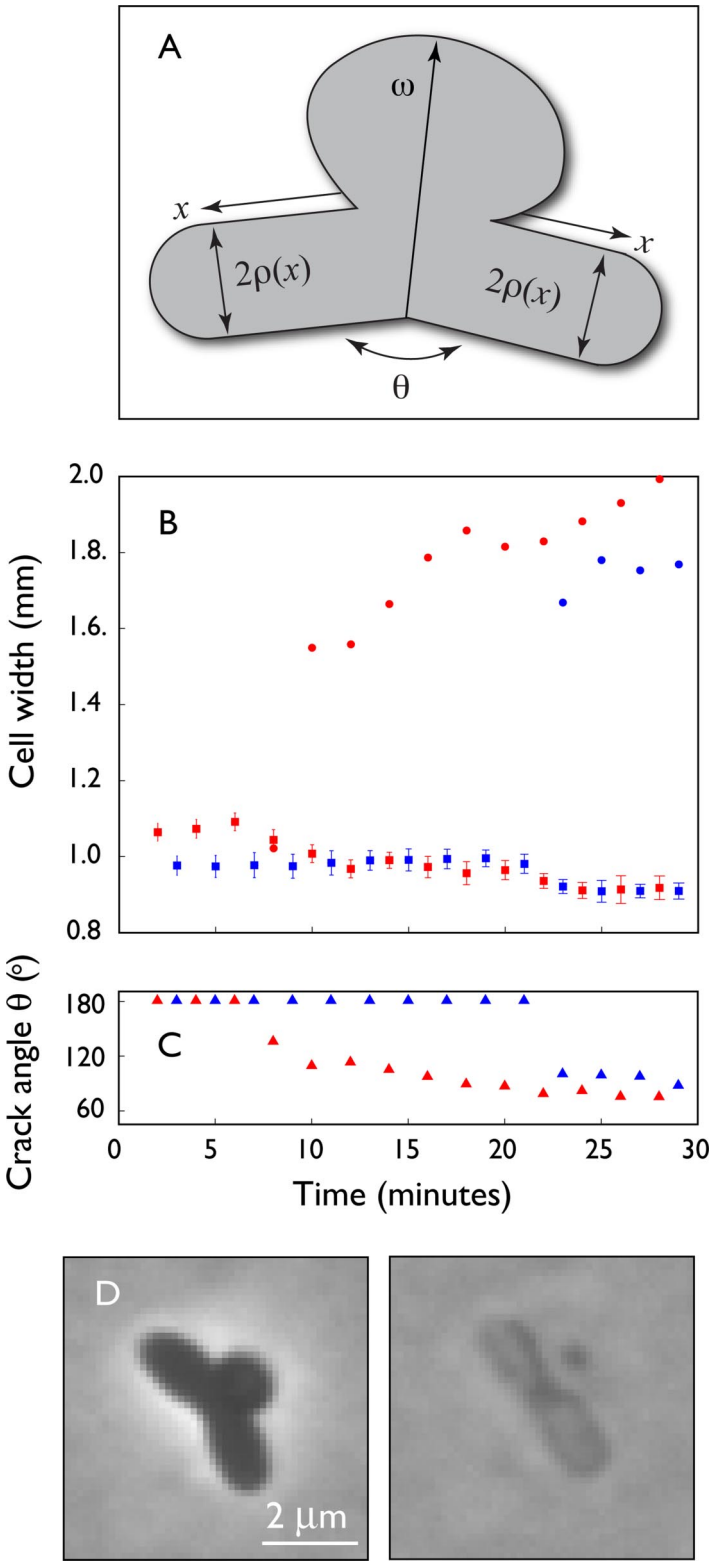

Fig. S4. Bulges cause only a local perturbation to cell shape. (*A*) The shape of a vancomycin-treated *imp4213 E. coli* cell with a typical bulge in the cell wall can be characterized by the cross-sectional diameter of the cell $2\rho(x)$, the bulge width ω, and the cracking angle θ. (*B*) The diameters (squares) of 2 typical cells (cell A from Fig. 2*A* in red, cell B from Fig. 2*E* in blue) remained approximately constant over time as the bulges grew, although there was a slight decrease in diameter when the bulges formed (at $t = 10$ min for cell A, $t = 23$ min for cell B), even as the bulge widths (circles) increased to twice the cell diameter. Error bars on the diameter were determined from 8 measurements taken roughly evenly along the cell length. The time $t = 0$ is arbitrary. (*C*) The cracking angle (triangles) decreased monotonically with the growth of the bulge. (*D*) Phase contrast of images directly before and after lysis of an *imp4213 E. coli* cell cracked around a midcell bulge. The bulge disappears after lysis, leaving a cylindrical husk.

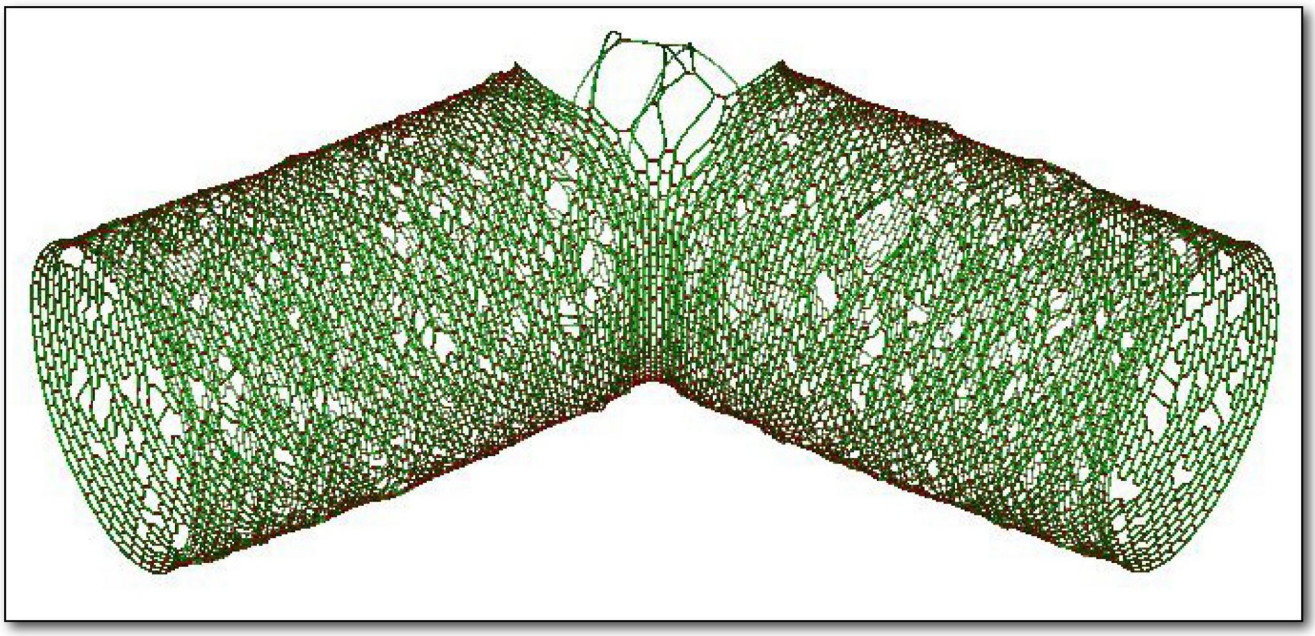

Fig. S5. Cracked cell with a realistic glycan strand-length distribution. The cracked shape of the model cell wall in Fig. 1*C* is essentially unaffected by the addition of the glycan defects from the topmost image of Fig. 3*B*, chosen such that the glycan strand-length distribution matches the experimental distribution in ref. 4.

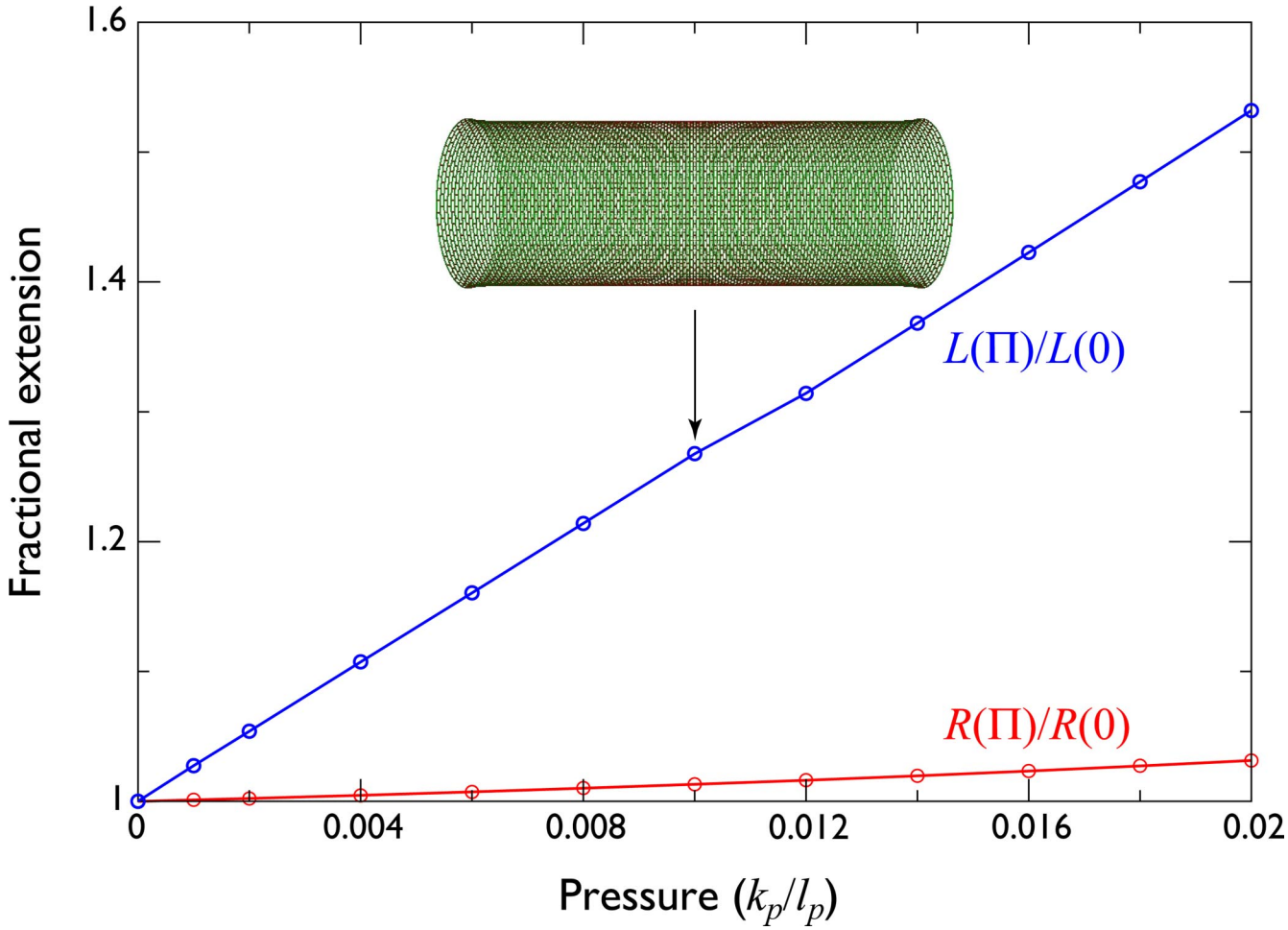

Fig. S6. Cell-wall dimensions depend linearly on turgor pressure. The length $L(\Pi)$ (shown in blue) and radius $R(\Pi)$ (red) are normalized to their values when the turgor pressure $\Pi = 0$. The cell wall and the arrow indicates the pressure used in the rest of this work, which corresponds to 1 atm for our chosen values of k_p and l_p.

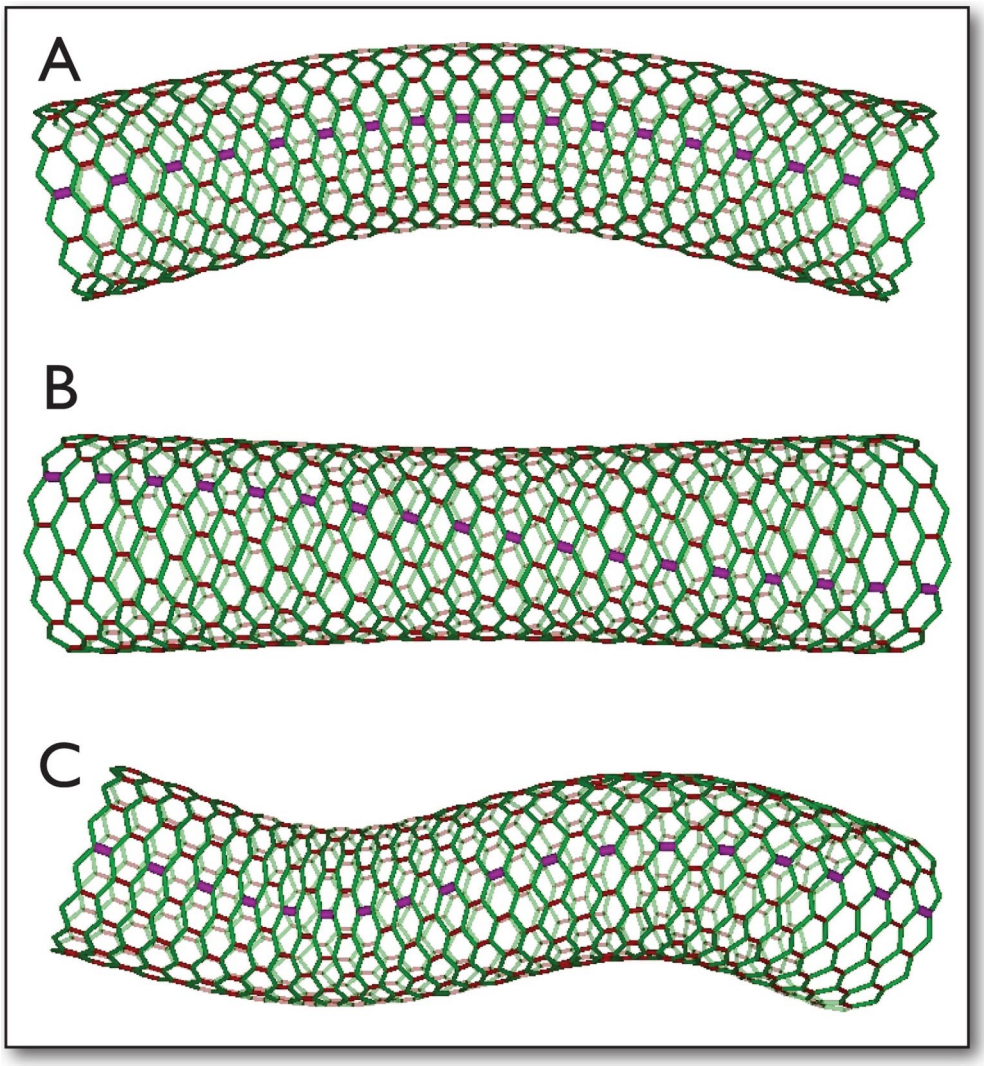

Fig. S7. Normal modes of a cylindrical peptidoglycan cell wall. Normal modes of the peptidoglycan network with the smallest eigenvalues (i.e., most easily excited modes). In each case, a line of peptides that are normally parallel are highlighted in purple. (*A*) Doubly degenerate bend mode. (*B*) Twist mode that wraps the lines of peptides around the cylinder. (*C*) Doubly degenerate higher-order bend mode.

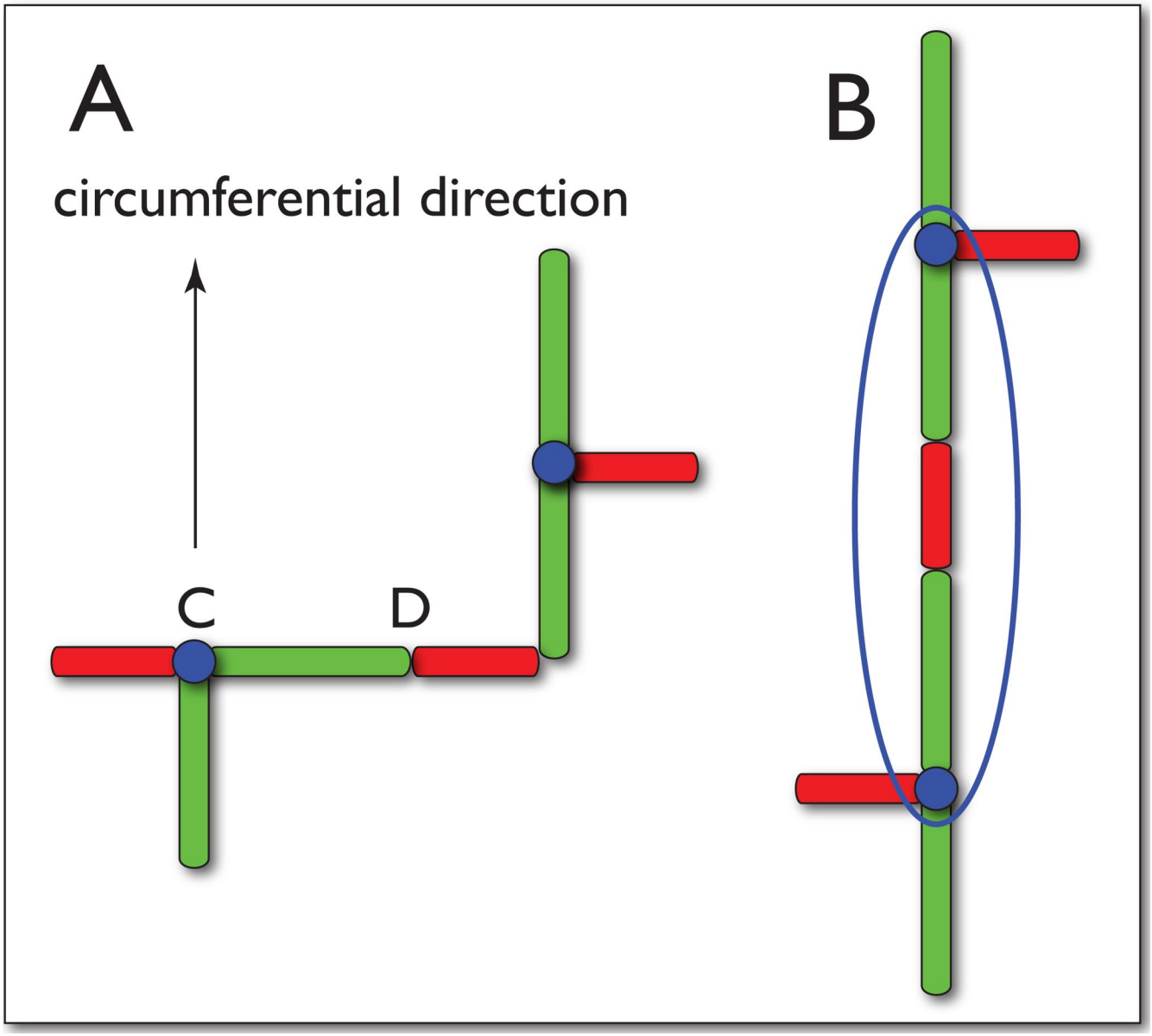

Fig. S8. Effect of misdirected glycan synthesis on cell-wall architecture. (*A*) Assume glycan synthesis initially follows the circumferential direction, but becomes misdirected between C and D and the glycan strand rotates to the longitudinal direction. The glycan strands are shown in their relaxed, linear state to emphasize the misdirection. The flexible peptide at the end of the glycan strand allows the longitudinal glycan to be crosslinked with the adjacent circumferential glycan strand. (*B*) When put under stress, the combined glycan strands will extend along the circumferential direction, thereby incorporating a peptide cross-link into the hoop. The glycan–peptide–glycan springs in the blue oval then act as an effective spring with a relaxed length $l_p + 2l_g$ and a spring constant of $k_p k_g/(2k_p + k_g)$, appropriate for springs in series.